Martínez-Haya, R.; Luna, MM.; Hijarro, A.; Martinez-Valero, E.; Miranda Alonso, MÁ.; Marín García, ML. (2019). Photocatalytic degradation of phenolic pollutants using N-methylquinolinium
and 9-mesityl-10-methylacridinium salts. Catalysis Today. 328:243-251.
https://doi.org/10.1016/j.cattod.2019.01.045

Photocatalytic Degradation of Phenolic Pollutants using *N*-Methylquinolinium and 9-Mesityl-10-methylacridinium salts

R. Martinez-Haya, M. M. Luna, A. Hijarro, E. Martinez-Valero, M.A. Miranda* and M. L. Marin*

Instituto de Tecnología Química, Universitat Politècnica de València-Consejo Superior de Investigaciones Científicas, Avda. de los Naranjos s/n, E-46022, Valencia, Spain

*Corresponding author

E-mail addresses: mmiranda@qim.upv.es; marmarin@qim.upv.es

Abstract

The photodegradation of a mixture of phenolic pollutants including: phenol (P), *orto*-phenylphenol (OPP), 2,4,6-trichlorophenol (TCP) and pentachlorophenol (PCP) was accomplished using two organic cationic photocatalysts, namely *N*-methylquinolinium (NMQ^+) and 9-mesityl-10-methylacridinium (Mes-Acr-Me^+) salts, due to their singular photophysical and redox properties. On one hand, NMQ^+ exhibits more energetic excited states and accordingly more favorable redox potentials than Mes-Acr-Me^+; on the other hand, NMQ^+ absorption reaches only up to 380 nm, while Mes-Acr-Me^+ extends in the visible up to 480 nm. A parallel evaluation of both photocatalysts, revealed that the highest level of photodegradation was achieved when they were employed at 20% mol. Specifically, with NMQ^+, removal of the pollutants was completed within 24 h of irradiation. Even more, irradiation time could be shortened from 24 to 8 hours, since high levels of removal were already achieved (93%, 100%, 100% and 82% for P, OPP, TCP and PCP, respectively). Yet, Mes-Acr-Me^+ was not as effective, and best results were obtained using 20 mol% upon 24 h of irradiation. Under these conditions, removal of PCP was 80%, while TCP was 40%, OPP 30% and P resulted in the most recalcitrant contaminant with only 10% of removal. Next, NMQ^+ and Mes-Acr-Me^+ were separately supported onto an inert inorganic support (Y-NMQ^+ and Y-Mes-Acr-Me^+), and elemental analyses revealed a loading of *ca*. 13% and 15% weight for NMQ^+ and Mes-Acr-Me^+, respectively. Upon heterogenization, in the case of Y-NMQ^+, the extent of removal was lower than the one achieved in the homogeneous photodegradations, for all the pollutants. Yet, the stability of Mes-Acr-Me^+ increased, and the removal of the pollutants resulted in better performance, thus within 48 h irradiation, 100% abatement of PCP, 50% of OPP and TCP and up to 40% of the most reluctant P, was achieved. Steady-state and time-resolved fluorescence quenching revealed that every pollutant was able to quench the

singlet excited state of both $^{1}(NMQ^{+})^{*}$ and $^{1}(Mes\text{-}Acr\text{-}Me^{+})^{*}$, with kinetic rate constants in the order of the diffusion limit. Thus, Type I photooxidation happening through the singlet excited state of either photocatalyst was the main operating process in the photodegradation of the studied pollutants.

Keywords: electron transfer; photocatalysis; singlet excited state; steady-state fluorescence; time-resolved fluorescence.

1. Introduction

Extensive agriculture is currently a motor of the economy for many countries; however, it is accompanied with several environmental problems such as massive use of pesticides, spoiled soils or use of huge volumes of water. In the Mediterranean area, production of olives accounts for approximately 63% of world production [1]. However, one of the main drawbacks associated with this industry is the great amount of wastewaters generated by olive oil production [2]. These wastewaters contain high concentrations of phenolic compounds, lipids, sugars and polyphenols [3]; therefore, they require specific pretreatments to prevent serious problems in the usual biological treatment processes.

Special attention has recently been paid to advanced oxidation processes (AOPs) to deal with the organic matter present in the wastewaters [4]. Among AOPs, photocatalysis constitutes an emerging green process with a proven potential for water remediation [5]. More specifically, organic photocatalysts offer the possibility of investigating the reaction mechanisms involved in photooxidation upon studying the reactivity of the photogenerated excited states by means of time-resolved techniques in the nano or micro-second scale [6].

With this background, the aim of the present work is to investigate the photodegradation of a mixture of phenolic pollutants (Figure 1) including: phenol (P), *orto*-phenylphenol (OPP), 2,4,6-trichlorophenol (TCP) and pentachlorophenol (PCP). They are generated in agriculture due to the widespread use of antifungals or pesticides [7]. To achieve the photodegradation of this group of pollutants, herein we have focused our attention on two organic cationic photocatalysts, namely *N*-methylquinolinium (NMQ^+) and 9-mesityl-10-methylacridinium ($Mes\text{-}Acr\text{-}Me^+$) salts, due to their singular photophysical and redox properties (Figure 2). Among their potential advantages as photocatalysts, they do not contain metals, and, being cationic, they should allow for efficient photoinduced electron

transfer, due to the lack of Coulombic attraction between the resulting species. Moreover, although both cations can generate singlet oxygen, previous results from our group have demonstrated that the contribution of this reacting oxygen species for the overall oxidation at typical pollutant concentrations is negligible compared to the photoinduced electron transfer pathway [8, 9]. Even more, although these photocatalysts are attracting some attention in the recent years [8], to the best of our knowledge, neither Mes-Acr-Me^+ nor related acridinium salts have been employed in pollutants treatment.

In spite of the fact that NMQ^+ and Mes-Acr-Me^+ share several advantages, there have certain properties that make them different enough to deserve a parallel evaluation. For instance, NMQ^+ exhibits more energetic singlet and triplet excited states than Mes-Acr-Me^+; this combined with the more favorable redox potentials makes NMQ^+ more attractive as Type I photocatalyst (Figure 2). Nevertheless, NMQ^+ absorption reaches only up to 380 nm, while Mes-Acr-Me^+ extends in the visible up to 480 nm (Figure S1). Whether one or the other parameter is more important would depend on the performance at the specific context and on the energetic and cost balances. Furthermore, while NMQ^+ has to be synthesized, Mes-Acr-Me^+ is commercially available.

Therefore, photodegradation of the mixture of phenolic pollutants has been evaluated in parallel with the two photocatalysts. In addition, both NMQ^+ and Mes-Acr-Me^+, have been supported onto zeolite Y-100 to investigate the abatement of pollutants in heterogeneous phase. Finally, a detailed time-resolved photophysical study has been undertaken to elucidate the operating mechanism.

2. Experimental

2.1. Chemicals

Phenol, *orto*-phenylphenol, 2,4,6-trichlorophenol, pentachlorophenol, *p*-xylene and 9-

mesityl-10-methylacridinium perchlorate were purchased from Sigma Aldrich. Zeolite Y 100 was obtained from Zeolyst International. Water used in electrochemical measurements and photodegradation experiments was Milli-Q grade; acetonitrile (ACN) was of HPLC quality from Scharlau and dimethyl sulfoxide (DMSO) was from Across. *N*-Methylquinolinium tetrafluoroborate salt was synthesized from quinoline (Sigma Aldrich) in two steps as previously described [10, 12]. Briefly, quinoline (0.42 mol) and methyl iodide (0.64 mol, 1.5 eq) were heated at 65 °C, under reflux for 24 h; afterwards, the resulting solid crude (*N*-methylquinolinium iodide) was washed with ether, for spectroscopic details see Figure S2. The solid *N*-methylquinolinium iodide was treated with $BF_3 \cdot Et_2O$ (2.6 eq) at 50 °C under stirring for 2.5 h, under nitrogen atmosphere. An additional amount of $BF_3 \cdot Et_2O$ (2.6 eq) was added and the mixture was stirred for further 2.5 h. The resulting solid was washed with ether and recrystallized from ethanol to yield *N*-methylquinolinium tetrafluoroborate, for the spectra see Figure S3.

Photocatalysts adsorption onto zeolite Y 100 was performed according to a previously described procedure [13]. Briefly, for the heterogeneization of NMQ^+ (Y-NMQ^+), Y-zeolite 100 (6.2 g) was suspended on an aqueous solution (25 mL) containing NMQ^+ tetrafluoroborate (1.0 g). The mixture was stirred and heated at 40 °C for 24 hours in the dark. Then, the solid was filtered, washed with water (30 mL) and dried at 100 °C for 72 h. Moreover, for the heterogeneization of Mes-Acr-Me^+ (Y-Mes-Acr-Me^+), Y-zeolite 100 (5 g) was suspended on a ACN:H_2O (1:1) solution (20 mL) containing Mes-Acr-Me^+ perchlorate (0.82 g). The mixture was stirred and heated at 40 °C for 24 hours in the dark. Then, the solid was filtered, washed with water (30 mL) and dried at 100 °C for 72 h. Loading of NMQ^+ and Mes-Acr-Me^+ on Y-NMQ^+ and Y-Mes-Acr-Me^+ were 13% wt and 15% wt, respectively, according to the elemental analysis.

2.2. Cyclic voltammetry

Cyclic voltammetric experiments were carried out using a cylindrical three-electrode quartz cell on a VersaSTAT 3 (Princeton Applied Research) electrochemical workstation with a glassy carbon (GCE) working electrode, a Pt wire counter electrode and a AgCl/Ag (sat KCl) as the reference electrode, in a one compartment electrochemical cell. The GCE and the Pt electrodes were polished using diamond spray (particle size 0.05 μm) before each experiment.

Stock solutions (1mM) of each pollutant were prepared in water:DMSO (24:1) for P, OPP and TCP, and in ACN for PCP. The cyclic voltammetries were carried out at room temperature, under a constant flux of N_2 using solutions of 30 μM of each pollutant in 0.1 M aqueous phosphate buffer pH 7 for P, OPP and TCP or in 0.1 M tetrabutyl ammonium perchlorate in ACN for PCP. The speed for the measurements was fixed at 0.05 $V \cdot s^{-1}$ The values of the redox potentials were calculated as the average between the maximum and minimum of the cyclic potential scan curves when the redox reactions were reversible, or from the maximum obtained in the voltammograms for the irreversible processes (Figure S4). The obtained data from the AgCl/Ag (sat KCl) were converted into redox potential values vs SCE as follows: E (vs SCE, in V) = E (vs AgCl/Ag, in V) -0.045 (Table S1).

2.3. Photocatalytic degradations

Homogeneous photochemical reactions were carried out in test tubes with magnetic stirring using a Luzchem photoreactor (model LZC-4 V) equipped with lamps emitting at 350 nm (9 bulbs) or 420 nm (7 bulbs), for NMQ^+ or Mes-Acr-Me^+, respectively. Aqueous solutions (9 mL) containing a mixture of the four pollutants (P, OPP, TCP and PCP, 5×10^{-5} M each) were irradiated under air, in the presence of different photocatalyst ratios (NMQ^+ or Mes-Acr-Me^+ at 1, 5, 10 or 20% mol). The removal of the pollutants at

different irradiation times was monitored by HPLC. The HPLC was an Agilent 1100 Series model with quaternary pump G1311A, photodiode detector VWD G1314A, standard liquid autosampler G1313A and degasser G1322A. A Mediterranea Sea 18 column (25 cm × 0.46 cm, 5 μm particle size) was employed. The mobile phase was fixed at 1.5 mL min^{-1} with an isocratic mixture of water pH 3 (30%) and acetonitrile (70%). To monitor removal of the pollutants, 100 μL of *p*-xilene (3.2×10^{-4} M ACN:H_2O (4:1)) were added as internal standard to every aliquot (500 μL), prior to injection. Then, aliquots of 90 μL were injected, and detection wavelength was fixed at 215 nm.

For the heterogeneous photoreactions, aqueous solutions of 15 mL containing a mixture of the four pollutants (5×10^{-4} M each) and supported catalyts at different ratios (13 and 26%mol for Y-NMQ^+ and 15 and 30%mol for Y-Mes-Acr-Me^+) were irradiated under air, using the above described Luzchem photoreactor. The removal of the pollutants was monitored by HPLC at different irradiation times as previously described for homogeneous photodegradations but filtering the sample before adding the internal standard with a 0.45 μm syringe filter.

2.4. Photophysical instrumentation

A Shimadzu UV-2101PC spectrophotometer was employed to obtain the UV/Vis absorption spectra of the photocatalysts (Figure S1) and the pollutants (Figure S5). Steady-state and time-resolved fluorescence experiments were performed with a Photon Technology International (PTI) LPS-220B spectrofluorometer and with a EasyLife V spectrofluorometer from OBB, respectively. In the case of time-resolved fluorescence, the excitation source was equipped with a pulsed LED (λ_{exc}=310 nm and 407 nm for NMQ^+ and Mes-Acr-Me^+, respectively); residual excitation signal was filtered in emission by using a cut-off filter (50% transmission at 320 nm and 435 nm for NMQ^+

and Mes-Acr-Me^+, respectively). Monoexponential decay functions that use a deconvolution procedure to separate them from the lamp pulse profile provided the fitted kinetic traces except in the case of NMQ^+ with OPP in which the decay function was adjusted to a biexponential relationship.

Photophysical measurements were run in solution (ACN:H_2O, 4:1 and in ACN for the UV spectra and for the fluorescence experiments, respectively), at room temperature, under nitrogen, using quartz cells of 1 cm optical path length. For the fluorescence quenching experiments, solutions of each photocatalyst with absorbance lower than 0.15 at λ_{exc}= 317 nm and 310 nm for NMQ^+ (steady-state and time-resolved, respectively), or 407 nm for Mes-Acr-Me^+, were treated with increasing concentrations of pollutant, up to 5.8 mM, 5.5 mM, 6.1 mM and 4.6 mM for P, OPP, TCP and PCP, respectively.

Diffuse reflectance of supported Zeolite Y-NMQ^+ and Zeolite Y-Mes-Acr-Me^+ were recorded using a Cary 5000 from Agilent Technologies. Solid emission fluorescence of supported Y-NMQ^+ and Y-Mes-Acr-Me^+ were recorded upon excitation at λ_{exc} = 340 nm and λ_{exc} = 420 nm nm for NMQ^+ and Mes-Acr-Me^+, respectively, and collected at 90° to minimize the scattered light (Figures S6 and S7).

3. Results

3.1. Homogeneous photochemical degradations

First, homogeneous photodegradation of aerobic aqueous mixtures of the four pollutants (P, OPP, TCP and PCP) in the presence of different molar ratios of each photocatalyst (1, 5, 10 and 20 mol%) was evaluated for 24 hours. Irradiation sources were centered at 350 nm or 420 nm, when using NMQ^+ or Mes-Acr-Me^+, respectively (Figures 3, S8 and S9). Comparing the activity of both photocatalysts, NMQ^+ was more efficient than Mes-Acr-Me^+ at every molar ratio. In both cases, the highest level of photodegradation was

achieved when photocatalyst was employed at 20% mol. Specifically, with NMQ^+, removal of the pollutants was completed within 24 h of irradiation. Even more, after 8 h of irradiation, high levels of removal were already achieved (93%, 100%, 100% and 82% for P, OPP, TCP and PCP, respectively), which suggests that irradiation time could be shortened from 24 to 8 hours. Yet, Mes-Acr-Me^+ was not as effective, and best results were obtained using 20 mol% upon 24 h of irradiation. Under these conditions, removal of PCP was 80%, while TCP was 40%, OPP 30% and P resulted in the most recalcitrant contaminant with only 10% of removal. From the irradiation mixtures, no clear-cut peaks were found in the HPLC analysis in any case, pointing out that under these conditions the pollutants disappear giving probably rise to a complex mixture of minor photoproducts, with insufficient individual concentrations to be detected.

Control experiments performed in the absence of light showed that the pollutants remain stable after equivalent reaction periods (Figure S10). Those carried out in order to check direct photolysis revealed that at 350 nm irradiation, direct absorption of light is partially responsible for the observed photodegradation, since it produced removal of PCP (up to 50%), P (40%), OPP (20%) and TCP (20%) (Figure S11); conversely, at 420 nm direct photolysis was almost negligible, in agreement with the UV spectra of the pollutants (Figure S5). Moreover, the stability of both photocatalysts was also monitored by UV absorption spectra (Figure S12). After 24 h of irradiation, the absorption spectrum of NMQ^+ kept the main bands, but their intensity decreased about 15%, whereas for the case of Mes-Acr-Me^+ a significant degradation was observed (about 60%). Therefore, the higher efficiency of NMQ^+ to produce the photodegradation of the mixture of pollutants is not only due to its higher redox potential compared to Mes-Acr-Me^+, but also to its higher photostability and to the contribution of direct photolysis at 350 nm.

3.2. Heterogeneous photochemical degradations

A typical strategy to improve the photostability and easy recovery of the photocatalysts that at the same time increases their potential for future applications involves heterogeneization, most commonly based on the adsorption of the organic compound onto a solid inert material, such as a zeolite [14-17]. For this purpose, NMQ^+ and Mes-Acr-Me^+ were separately supported onto an inert inorganic support (zeolite Y 100), elemental analysis of the new materials (Y-NMQ^+ and Y-Mes-Acr-Me^+) revealed a loading of *ca*. 13% and 15% weight for NMQ^+ and Mes-Acr-Me^+, respectively. Moreover, diffuse reflectance and fluorescence emission spectra (Figures S6 and S7) demonstrated that incorporation of the photocatalysts onto the zeoliteas shown by the presence of the absorption and emission bands of the chromophores.

Next, to evaluate the performance of Y-NMQ^+ and Y-Mes-Acr-Me^+, new mixtures of the pollutants (5×10^{-4} M each) in aerobic DMSO:H_2O (30:70) media, were irradiated under aerated atmosphere, using 350 nm centered light in the presence of Y-NMQ^+, or 420 nm centered light in the presence of Y- Mes-Acr-Me^+ (Figures 4 and S13). Two different molar ratios were tested (13 and 26 mol% for Y-NMQ^+, and 15 and 30 mol% for Y-Mes-Acr-Me^+), and in every case higher ratio of heterogeneous photocatalysts resulted in higher percentages of contaminants abatement. Control experiments to check the adsorption of the pollutants onto the zeolites Y-NMQ^+ and Y- Mes-Acr-Me^+ indicated that it was lower than 10%, therefore the observed photodegradation was safely attributed to the photocatalyzed degradation. In the case of Y-NMQ^+, the extent of removal was lower than the one achieved in the homogeneous photodegradations for all the pollutants, even with longer irradiation times. Nevertheless, for the case of Y-Mes-Acr-Me^+, heterogeneization resulted in better performance, thus within 48 h irradiation, 100% abatement of PCP, 50% of OPP and TCP and up to 40% of the most reluctant P, was

achieved. For Y-Mes-Acr-Me$^+$, evolution of the pollutants removal with time revealed two different trends, at the beginning, the removal rate for all the pollutants was similar; however, after 5 hours irradiation the photodegradation slowed down, and different degrees of removal were observed upon 48 h. This fact reveals that upon heterogeneization, the photostability of Y-Mes-Acr-Me$^+$ increased, and accordingly, efficiency was also improved.

3.3 Thermodynamic feasibility of the redox processes

As mentioned above, although NMQ$^+$ and Mes-Acr-Me$^+$ are able to generate singlet oxygen [8, 11], at the employed pollutant concentration photoinduced electron transfer must be responsible for the observed photodegradations (Scheme 1). Nevertheless, a thermodynamic analysis of the potential participation of the singlet excited state of the photocatalysts can be performed using the photoinduced Gibbs free energy (eq. 1) [18], the experimentally measured redox potentials values (Figure S4, and table S1) and the energy of the excited states (Figure 2).

$$\Delta G^o_{et} = -\left[E^o_{red}\left(PC^+/PC^{\cdot}\right) - E^o_{red}\left(Q^{\cdot+}/Q\right)\right] - E^*_{PC^+} \quad \text{(eq. 1)}$$

where PC$^+$ represents NMQ$^+$ and Mes-Acr-Me$^+$ and Q is any pollutant.

Table 1 reveals that photooxidative degradations are exergonic for both photocatalysts acting from their singlet excited states. To close the photocatalytic cycle, formation of superoxide anion from the reduction of O_2 (E^o_{red} = -0.33 V vs SCE) [19] would be exergonic in both cases (-0.52 eV and -0.16 eV for NMQ$^+$ and Mes-Acr-Me$^+$, respectively).

The obtained values reveal that, as expected, singlet excited states of both photocatalysts could, in principle, participate in the photoinduced electron transfer. Nevertheless, it is mandatory to perform kinetic studies to evaluate the viability of the electron transfer in

the time scale of those excited states.

3.4. Fluorescence quenching studies

Therefore, steady-state and time resolved fluorescence measurements were carried out in order to determine the participation of the singlet excited state of the photocatalysts in the removal of the contaminants, see Figures 5 and 6. From these experiments it is clear that every pollutant is able to quench the singlet excited state of both $^{1}(NMQ^{+})^{*}$ and ^{1}(Mes-Acr-Me^{+})*. Special attention is required to the case of the quenching of $^{1}(NMQ^{+})^{*}$ by OPP (Figure 5B left). The new band observed upon addition of OPP corresponds to the emission of OPP, obtained from the partial direct excitation of OPP at 317 nm. Therefore, the time-resolved measurements required a two-exponential fitting of the decay (see Figure 5B right). Table 2 revels an efficient kinetic quenching constants between the pollutants and the singlet excited states of each photocatalyst from both sets of measurements, with values close to the diffusion limit (in the order of 10^{10} $M^{-1}s^{-1}$) [20].

3.5. Mechanistic proposal

Scheme 2 shows the postulated mechanism to explain photooxidation of the phenolic pollutants. Quenching of the singlet excited states resulted to be dynamic acting as a proof of the participation of these excited states in the photoinduced electron transfer. Thus, Type I photooxidation happening through the singlet excited state of either photocatalyst is the main operating process in the photodegradation of the studied pollutants.

Conclusions

Homogeneous photodegradation of phenolic compounds can be efficiently achieved with both photocatalysts, NMQ^{+} and Mes-Acr.-Me^{+}; however, the rate of the process depends

on the nature of the photocatalyst. Thus, the highly oxidizing NMQ^+ leads to higher degradation levels, which in part is due to direct photolysis. In the case of Mes-Acr-Me^+, its lower redox potential and photostability results in a reduced photoactivity and therefore in a slower degradation; however, its capability to absorb visible light may be advantageous for environmental applications. After heterogenization, the stability of Mes-Acr-Me^+ increases and the removal of the pollutants becomes more efficient. Steady-state and time resolved fluorescence quenching reveal that both photocatalysts are capable of oxidizing the pollutants from their singlet excited states, with kinetic rate constants in the order of the diffusion limit.

Acknowledgements

Financial support from Spanish Government (Grants SEV-2016-0683) is gratefully acknowledged. We also thank support from VLC/Campus. R. Martinez-Haya thanks financial support for a predoctoral contract from Apadrina la Ciencia Association and Ford España/Ford Motor Company Fund.

References

[1] G. Banias, C. Achillas, C. Vlachokostas, N. Moussiopoulos, M. Stefanou, Environmental impacts in the life cycle of olive oil: a literature review, J. Sci. Food Agric., 97 (2017) 1686-1697.
[2] M. Beccari, F. Bonemazzi, M. Majone, C. Riccardi, Interaction between acidogenesis and methanogenesis in the anaerobic treatment of olive oil mill effluents, Water Research, 30 (1996) 183-189.
[3] N. Adhoum, L. Monser, Decolourization and removal of phenolic compounds from olive mill wastewater by electrocoagulation, Chemical Engineering and Processing: Process Intensification, 43 (2004) 1281-1287.
[4] C. Amor, M.S. Lucas, J. García, J.R. Dominguez, J.B. De Heredia, J.A. Peres, Combined treatment of olive mill wastewater by Fenton's reagent and anaerobic biological process, Journal of Environmental Science and Health, Part A, 50 (2015) 161-168.
[5] S. Malato, P. Fernandez-Ibanez, M.I. Maldonado, J. Blanco, W. Gernjak, Decontamination and disinfection of water by solar photocatalysis: Recent overview and trends, Catal. Today, 147 (2009) 1-59.

[6] M.L. Marin, L. Santos-Juanes, A. Arques, A.M. Amat, M.A. Miranda, Organic photocatalysts for the oxidation of pollutants and model compounds, Chem. Rev., 112 (2012) 1710-1750.
[7] M.A. Miranda, F. Galindo, A.M. Amat, A. Arques, Pyrylium salt-photosensitised degradation of phenolic contaminants present in olive oil wastewaters with solar light: Part II. Benzoic acid derivatives, Appl. Catal. B, 30 (2001) 437-444.
[8] R. Martinez-Haya, C. Sabater, M.-Á. Castillo, M.A. Miranda, M.L. Marin, A mechanistic study on the potential of quinolinium salts as photocatalysts for the abatement of chlorinated pollutants, J. Hazard. Mater., 351 (2018) 277-284.
[9] R. Martinez-Haya, M.A. Miranda, M.L. Marin, Type I vs Type II photodegradation of pollutants, Catal. Today, 313 (2018) 161-166.
[10] U.C. Yoon, S.L. Quillen, P.S. Mariano, R. Swanson, J.L. Stavinoha, E. Bay, Exploratory and Mechanistic Aspects of the Electron-Transfer Photochemistry of Olefin-N-Heteroaromatic Cation Systems, J. Am. Chem. Soc., 105 (1983) 1204-1218.
[11] A.C. Benniston, A. Harriman, P. Li, J.P. Rostron, H.J. van Ramesdonk, M.M. Groeneveld, H. Zhang, J.W. Verhoeven, Charge shift and triplet state formation in the 9-mesityl-10-methylacridinium cation, J. Am. Chem. Soc., 127 (2005) 16054-16064.
[12] P.F. Donovan, D.A. Conley, Some organic tetrafluoroborates, J. Chem. Eng. Data, 11 (1966) 614-&.
[13] A. Arques, A.M. Amat, L. Santos-Juanes, R.F. Vercher, M.L. Marin, M.A. Miranda, Abatement of methidathion and carbaryl from aqueous solutions using organic photocatalysts, Catal. Today, 144 (2009) 106-111.
[14] V. Ramamurthy, J.V. Caspar, D.R. Corbin, Generation, entrapment, and spectroscopic characterization of radical cations of .alpha.,.omega.-diphenyl polyenes within the channels of pentasil zeolites, J. Am. Chem. Soc., 113 (1991) 594-600.
[15] F. Gessner, J.C. Scaiano, Intrazeolite photochemistry VII: Laser photolysis of stilbene and some aromatic hydrocarbons in the cavities of NaX zeolite studied by time-resolved diffuse reflectance, J. Photochem. Photobiol., A, 67 (1992) 91-100.
[16] S. Sankararaman, K.B. Yoon, T. Yabe, J.K. Kochi, Control of back electron transfer from charge-transfer ion pairs by zeolite supercages, J. Am. Chem. Soc., 113 (1991) 1419-1421.
[17] A.M. Amat, A. Arques, S.H. Bossmann, A.M. Braun, S. Gob, M.A. Miranda, A "Camel through the eye of a needle": Direct introduction of the TPP+ ion inside Y-zeolites by formal ion exchange in aqueous medium, Angew. Chem., Int. Ed., 42 (2003) 1653-1655.
[18] D. Rehm, A. Weller, Kinetics of fluorescence quenching by electron and H-atom transfer, Isr. J. Chem., 8 (1970) 259-271.
[19] Y.A. Ilan, D. Meisel, G. Czapski, The Redox Potential of the O2–O−2 System in Aqueous Media, Isr. J. Chem., 12 (1974) 891-895.
[20] S.L. Murov, I. Carmichael, G.L. Hug, Handbook of Photochemistry, 2nd ed., Marcel Dekker, New York, 2009.

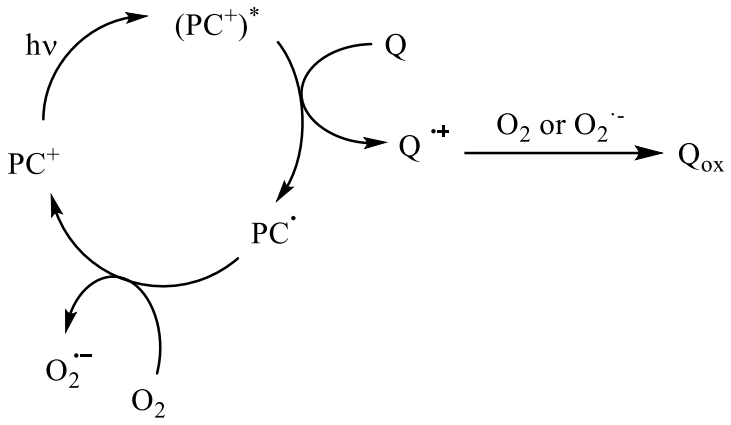

Scheme 1

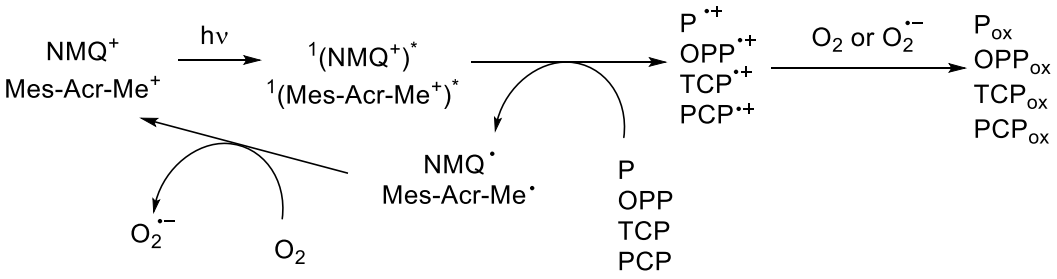
NMQ+
Mes-Acr-Me+
hν
1(NMQ+)*
1(Mes-Acr-Me+)*
P •+
OPP•+
TCP•+
PCP•+
O2 or O2•–
Pox
OPPox
TCPox
PCPox
NMQ•
Mes-Acr-Me•
P
OPP
TCP
PCP
O2•–
O2

Scheme 2

Table 1

Pollutant	ΔG_{et}^{o} NMQ^{+} (eV)	ΔG_{et}^{o} Mes-Acr-Me^{+} (eV)
P	-2.04	-1.52
OPP	-1.55	-1.03
TCP	-1.57	-1.05
PCP	-1.03	-0.51

Table 2

	k_q ($M^{-1}s^{-1}$)			
	$^1(NMQ^+)^*$	$^1(NMQ^+)^*$	$^1(Mes\text{-}Acr\text{-}Me^+)^*$	$^3(Mes\text{-}Acr\text{-}Me^+)^*$
	steady-state	time-resolved	steady-state	time-resolved
P	2.7×10^{10}	1.6×10^{10}	1.5×10^{10}	7.7×10^{9}
OPP	2.7×10^{10}	4.8×10^{10}	1.5×10^{10}	7.5×10^{9}
TCP	2.1×10^{10}	1.1×10^{10}	4.1×10^{9}	2.4×10^{9}
PCP	8.6×10^{10}	8.7×10^{9}	5.2×10^{8}	1.4×10^{9}

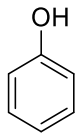

Phenol
(**P**)

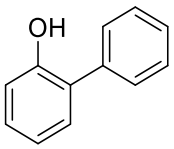

orto-Phenylphenol
(**OPP**)

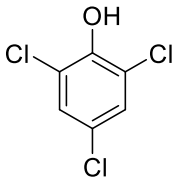

2,4,6-Trichlorophenol
(**TCP**)

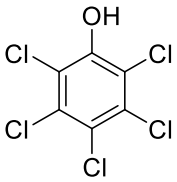

Pentachlorophenol
(**PCP**)

Figure 1

	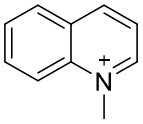	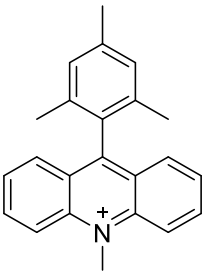
	N-methylquinolinium (**NMQ**$^+$)[6, 10]	9-Mesityl-10-methylacridinium (**Mes-Acr-Me**$^+$)[11]
E_{red} (V vs SCE)	-0.85	-0.49
E^*_S (eV)	3.55	2.67
E^*_T (eV)	2.65	1.94
τ_S (ns)	20	6.0
τ_T (μs)	-	30
Φ_Δ	0.85	0.42

Figure 2

(A) (B)

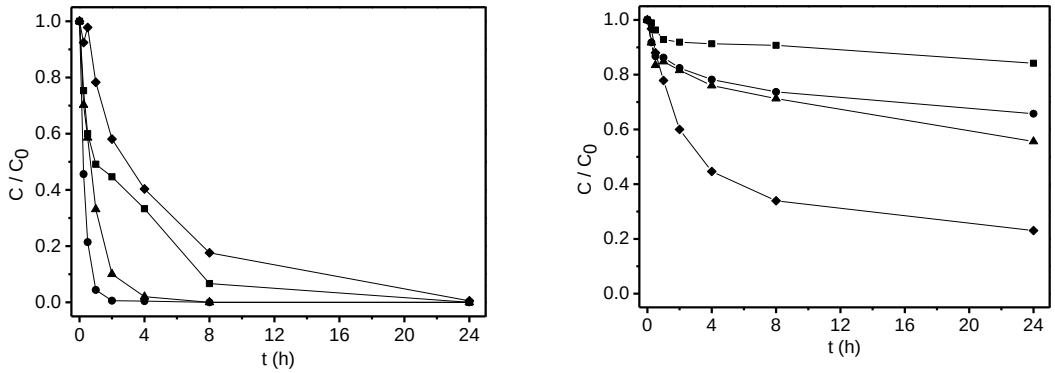
1.0
0.8
0.6
0.4
0.2
0.0
C / C0
0
4
8
12
16
20
24
t (h)
1.0
0.8
0.6
0.4
0.2
0.0
C / C0
0
4
8
12
16
20
24
t (h)

Figure 3

(A) (B)

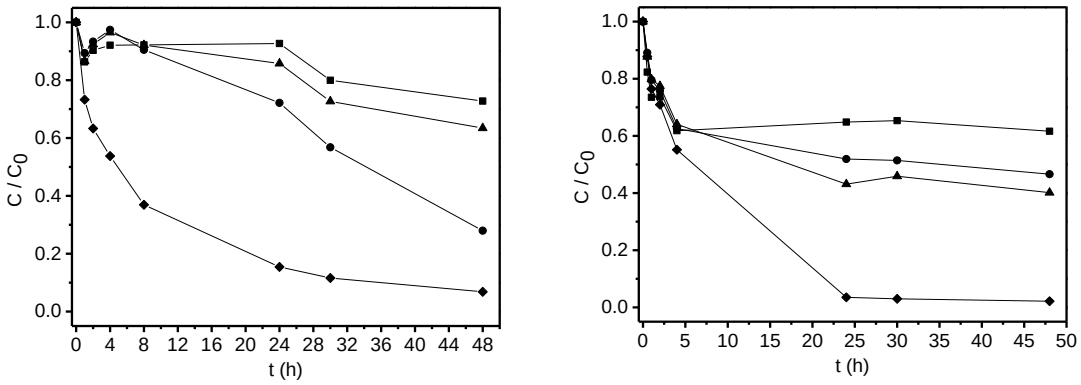
1.0
0.8
0.6
0.4
0.2
0.0
C / C0
0 4 8 12 16 20 24 28 32 36 40 44 48
t (h)
1.0
0.8
0.6
0.4
0.2
0.0
C / C0
0 5 10 15 20 25 30 35 40 45 50
t (h)

Figure 4

(A)

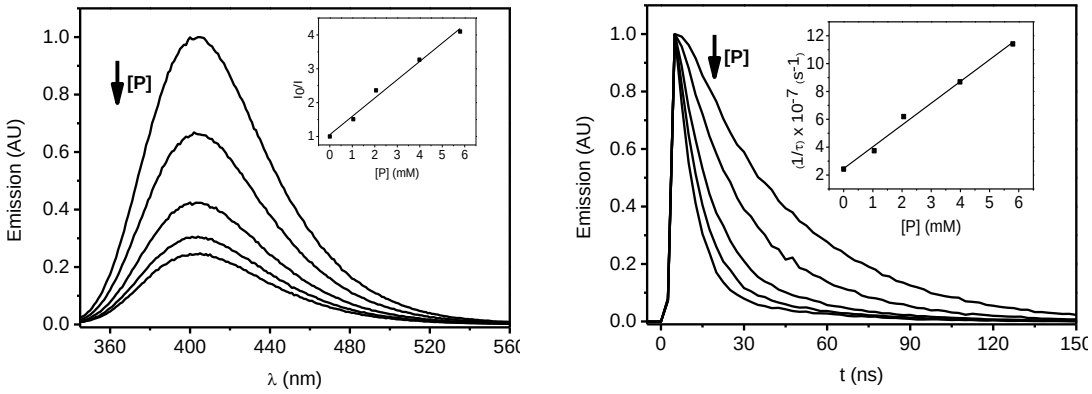
[P]
Emission (AU)
λ (nm)
Io/I
[P] (mM)
[P]
t (ns)
(1/τ) x 10^-7 (s^-1)
[P] (mM)

(B)

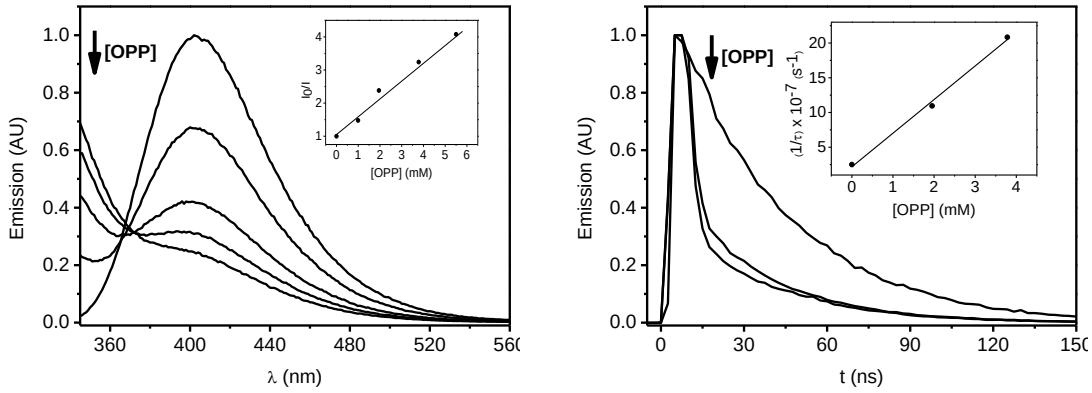
[OPP]
Emission (AU)
λ (nm)
Io/I
[OPP] (mM)
[OPP]
t (ns)
(1/τ) x 10^-7 (s^-1)
[OPP] (mM)

(C)

(D)

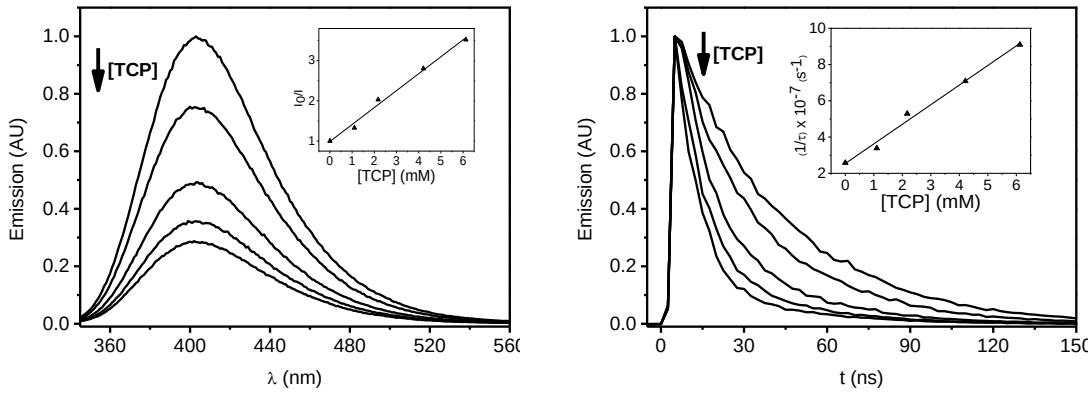
[TCP]
Emission (AU)
λ (nm)
Io/I
[TCP] (mM)
[TCP]
t (ns)
(1/τ) x 10^-7 (s^-1)
[TCP] (mM)

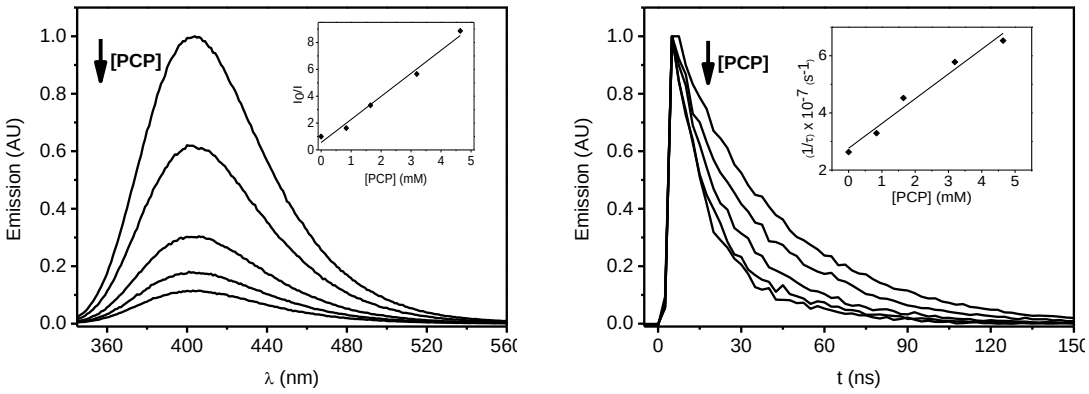
[PCP]
Emission (AU)
λ (nm)
I0/I
[PCP] (mM)
[PCP]
Emission (AU)
t (ns)
(1/τ0 x 10-7 (s-1)
[PCP] (mM)

Figure 5

(A)

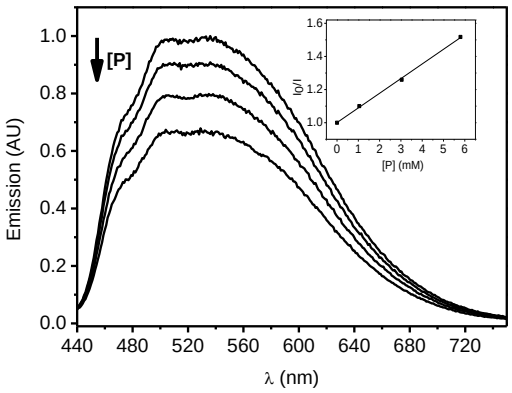
[P]
Emission (AU)
λ (nm)
I0/I
[P] (mM)

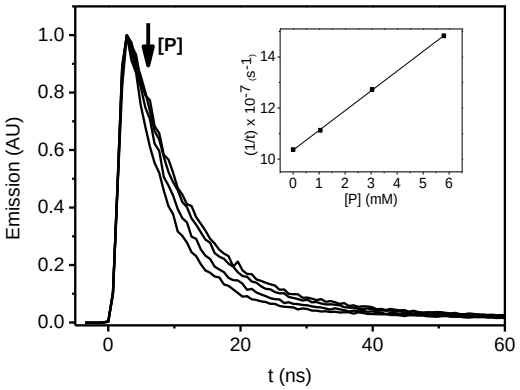
[P]
Emission (AU)
t (ns)
(1/τ) x 10^-7 (s^-1)
[P] (mM)

(B)

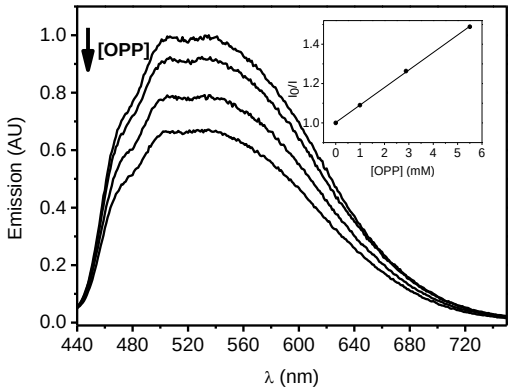
[OPP]
Emission (AU)
λ (nm)
I0/I
[OPP] (mM)

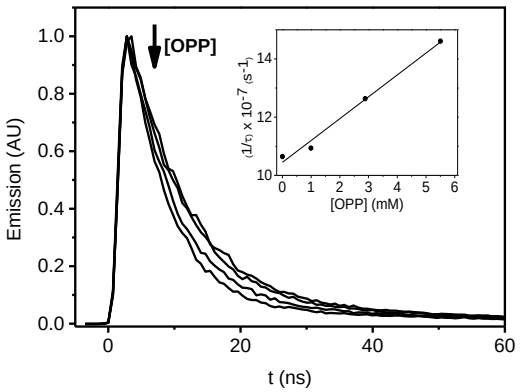
[OPP]
Emission (AU)
t (ns)
(1/τ) x 10^-7 (s^-1)
[OPP] (mM)

(C)

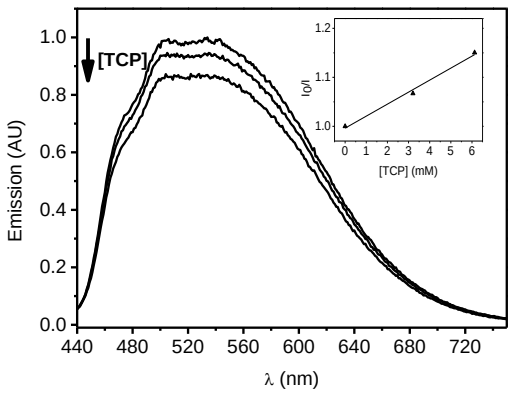
[TCP]
Emission (AU)
λ (nm)
I0/I
[TCP] (mM)

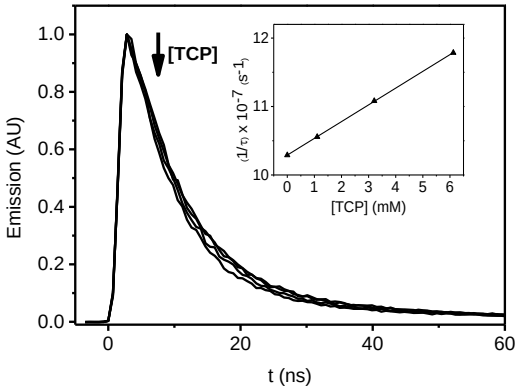
[TCP]
Emission (AU)
t (ns)
(1/τ) x 10^-7 (s^-1)
[TCP] (mM)

(D)

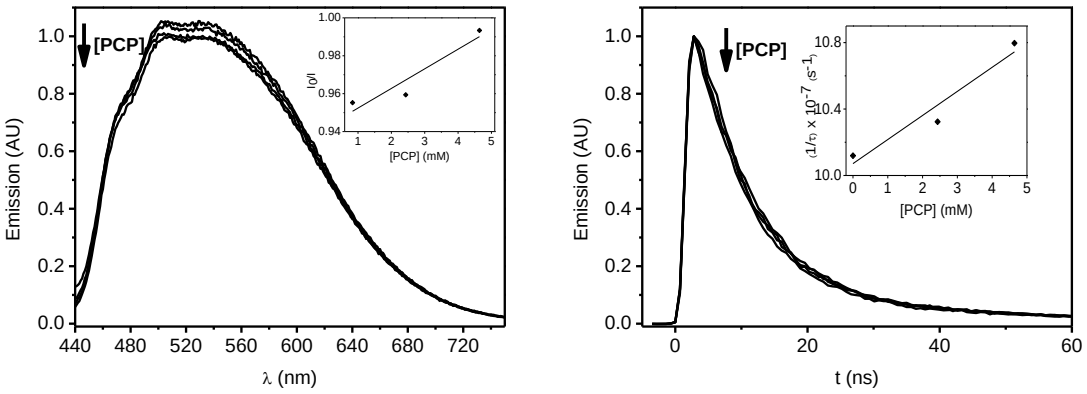
[PCP]
Emission (AU)
λ (nm)
I0/I
[PCP] (mM)
[PCP]
Emission (AU)
t (ns)
(1/τ0) x 10-7 (s-1)
[PCP] (mM)

Figure 6

CAPTIONS FOR SCHEMES, TABLES AND FIGURES

Scheme 1. Photoredox catalytic cycle of NMQ^+ and Mes-Acr-Me^+ (represented as PC^+) involving photooxidation of the pollutants (Q).

Scheme 2. Potential mechanistic pathway to explain the photooxidation of the pollutants.

Table 1. Estimated free energy changes for the photoinduced electron transfer from the pollutants to the singlet excited state of each photocatalyst, calculated according to (eq. 1).

Table 2. Rate constant values for the reaction between the pollutants and NMQ^+ and Mes-Acr-Me^+ obtained from steady-state and time-resolved experiments.

Figure 1. Chemical structures of the selected pollutants.

Figure 2. Chemical structures, redox and photophysical properties of NMQ^+ and Mes-Acr-Me^+.

Figure 3. Plot of the relative concentration of P (■), OPP (●), TCP (▲) and PCP (♦) at initial global concentration of $C_0 = 2 \times 10^{-4}$ M *vs* 350 nm irradiation time in the presence of 20 mol% NMQ^+ (A) or 420 nm irradiation in the presence of 20 mol% Mes-Acr-Me^+ (B) under aerated atmosphere in aqueous media.

Figure 4. Plot of the relative concentration of P (■), OPP (●), TCP (▲) and PCP (♦) at initial global concentration of $C_0 = 2 \times 10^{-3}$ M *vs* irradiation time in aerated DMSO:H_2O (30:70) media, irradiated at 350 nm in the presence of Y-NMQ^+ (26 mol%)(A) and at 420 nm in the presence of Y-Mes-Acr-Me^+ (30 mol%) (B).

Figure 5. Steady-state (left column) and time-resolved (right column) $^1(NMQ^+)^*$ fluorescence quenching upon addition of increasing concentrations of P (A), OPP (B), TCP (C) and PCP (D) in ACN under N_2; λ_{exc} = 310 nm. Insets: Stern Volmer plots obtained from the corresponding steady-state (left) and time-resolved (right) experiments.

Figure 6. Steady-state (left column) and time-resolved (right column) $^{1}(\text{Mes-Acr-Me}^{+})^{*}$ fluorescence quenching upon addition of increasing concentrations of P (A), OPP (B), TCP (C) and PCP (D) in ACN under N_2; λ_{exc} = 310 nm. Insets: Stern Volmer plots obtained from the corresponding steady-state (left) and time-resolved (right) experiments.